American Mineralogist, Volume 92, pages 994–1006, 2007

Dehydration of Ca-montmorillonite at the crystal scale. Part I: Structure evolution

Eric Ferrage,* Caroline A. Kirk, Gordon Cressey, and Javier Cuadros

The Natural History Museum, Department of Mineralogy, Cromwell Road, London SW7 5BD, U.K.

Abstract

The dehydration dynamics of the of the Ca-saturated <1 μm size fraction of SWy-1 (low-charge montmorillonite) were studied at the crystal scale under isothermal conditions using X-ray diffraction with a position-sensitive detector (XRD-PSD) in the 30–170 °C temperature range. A total of 630 XRD patterns were modeled between 30 and 125 °C using a trial-and-error approach based on the direct comparison of experimental and calculated XRD patterns. The proportion of layers with different hydration states (bihydrated, mono-hydrated, and dehydrated) were determined in the temperature-time space as well as small variations of layer thickness within each hydration state. The results showed that dehydration produces complex structures with heterogeneous hydration states, some of which are stable (not transient) and remain at the end of the experiment. The evolution of other structural parameters (interlayer water content, layer thickness fluctuation) was consistent with previous reports of smectite hydration. For bihydrated layers, the amount of water molecules per interlayer cation indicated the presence of water molecules both coordinated and non-coordinated to the interlayer cation. The transition from bi- to mono-hydrated layers produced the maximum structural heterogeneity, with (1) strong interlayer thickness fluctuation (in individual layers), and (2) the presence of several elementary mixed-layer structures. In contrast, the transition from mono-hydrated to dehydrated layers occurs homogeneously within layers. Finally, the decrease in thickness of mono-hydrated layers only implied the removal of some water molecules forming the hydration shell of the interlayer cation.

Keywords: Crystal structure, smectite-water, diffusion, water in smectite interlayer, order-disorder, mixed-layering, XRD data, smectite, montmorillonite

Introduction

Smectite is a clay mineral that occurs in many surface environments, both terrestrial and marine, frequently as one of the main mineral components. The expandability properties of its interlayer space and the resulting large surface area make it a main control of the physical and chemical behavior of the environments where it is found. Thus smectite is important in many applications; e.g., in agriculture (to retain and release water and nutrients), in civil engineering (for controlling ground properties), for industrial applications (making use of the large active surface area), in the construction of waste repositories (providing impermeable barriers to retain pollutants), including those for nuclear waste containment, etc. However, as smectite reacts quickly to changing environmental conditions, it can display a wide range of structural states that can depend strongly on cation exchange, temperature, or relative humidity (RH). Such modifications involve differences in hydration/dehydration states that can alter significantly the properties of smectite. Indeed, the change in volume that results from dehydration can cause a dramatic modification of the bulk texture of the material, induce the formation of cracks, and lead to a strong alteration of water migration paths. Thus dehydration will reduce the efficiency of a smectite waste barrier and could lead to fluid and pollutant flows in and out of a repository. In this respect, the establishment of a realistic model of smectite behavior requires a good understanding of the organization of water and its hydration/dehydration mechanism occurring at each scale of observation. At the crystal scale, smectite structure most often exhibits, within the same crystallite, layers with different interlayer water configurations (Cases et al. 1992, 1997; Bérend et al. 1995; Cuadros 1997; Calarge et al. 2003; Ferrage 2004; Michot et al. 2005; Ferrage et al. 2005a, 2005b, 2007). This effect can be quantified by comparing X-ray diffraction (XRD) profiles with patterns calculated assuming a random interstratification of layers exhibiting different hydration states (Ferrage 2004; Ferrage et al. 2005a, 2005b, 2007).

This paper reports on a detailed characterization of the structural dehydration process of a calcium-saturated low-charge montmorillonite reference sample (The Clay Mineral Society Source Clay, SWy-2). In part I of the present study, we assess the evolution of the smectite structure subjected to dehydration between 25–125 °C by systematically comparing the experimental XRD patterns with calculated models, to obtain the proportion of layers with defined hydration states. Additional structural parameters, such as the thickness of hydrated layers and the water content, are also assessed. The obtained evolution of structural parameters will be used in part II of this paper to propose a kinetic model of smectite dehydration that can be used for the prediction of structural changes of this mineral.

* E-mail: e.ferrage@nhm.ac.uk

0003-004X/07/0007–994$05.00/DOI: 10.2138/am.2007.2396

Background

The ability of smectites to incorporate interlayer H_2O molecules and the subsequent change in basal spacing has been extensively studied for several decades. For example, XRD studies (Nagelschmidt 1936; Bradley et al. 1937; Mooney et al. 1952; Méring and Glaeser 1954; Norrish 1954) showed that the basal spacing of smectite increases in steps as a function of the relative humidity, corresponding to the intercalation of 1, 2, or 3 planes of H_2O molecules in the smectite interlayer. From these pioneering studies, several possible models have been proposed in which crystalline swelling is controlled by the balance of repulsive forces between the negatively charged layers and attractive forces between the hydrated interlayer cations and the layers (Norrish 1954; Van Olphen 1965; Kittrick 1969a, 1969b; Laird 1996, 1999).

Smectite hydration state is often characterized by XRD using the evolution of the (001) basal-spacing under variable RH (Méring and Glaeser 1954; Harward and Brindley 1965; Glaeser et al. 1967; Glaeser and Méring, 1968; Harward et al. 1969; Watanabe and Sato 1988; Sato et al. 1992; Yamada et al. 1994; Tamura et al. 2000; Ferrage 2004; Ferrage et al. 2005a, 2005b, 2007, among others). This technique is useful when most layers in the structure are either dehydrated (0W = 9.7–10.2 Å), mono-hydrated (1W = 11.6–12.9 Å), or bihydrated (2W = 14.9–15.7 Å). However the coexistence of different hydration states in a sample is common even under controlled conditions (Méring and Glaeser 1954; Glaeser et al. 1967; Glaeser and Méring 1968; Sato et al. 1992, 1996). For example, the irrational character of the (00*l*) reflection series at the transition between two discrete hydration states and the asymmetric peak profiles (Sato et al. 1992) are evidence of this coexistence. Few studies have taken into account the coexistence of layers with contrasting layer thickness corresponding to different hydration states by using an XRD profile modeling approach (Moore and Hower 1986; Iwasaki and Watanabe 1988; Bérend et al. 1995; Cases et al. 1997; Cuadros 1997). More recently, Ferrage (2004) and Ferrage et al. (2005a, 2005b, 2007) have applied successfully XRD profile modeling by fitting both positions and profiles of the 00*l* reflections over a large angular range, and this approach showed that randomly interstratified structures, each containing different layer types, coexist systematically in these smectite samples over a wide range of RH. The heterogeneity of charge distribution is sometimes made responsible for the hydration heterogeneity observed (Sato et al. 1992; Calarge et al. 2003). However, the hydration heterogeneity also observed by Ferrage (2004) for synthetic smectites with an assumed homogeneous charge distribution may indicate that this phenomenon is an intrinsic property of smectite structure. Because this effect complicates the determination of structural features and because smectite responds rapidly to changing external conditions, the influence of temperature on the crystal structure of smectite is not well documented. Bray et al. (1998) attempted to study dynamic and isothermal dehydration of montmorillonite using synchrotron source X-rays. These authors observed a modification in peak position and width suggesting the presence of mixed-layering but did not attempt to derive a kinetic model for structural dehydration.

Most studies relating to the influence of temperature on smectite dehydration have been performed using thermogravimetric or differential thermal analysis (Hendricks et al. 1940; Mackenzie 1950, 1952; Poinsignon et al. 1982; Guindy et al. 1985; Girgis et al. 1987; Laureiro et al. 1996; Bray et al. 1998; Bray and Redfern 1999; Zabat and Van Damme 2000). Many of these studies showed that dehydration occurs non-uniformly, with defined discrete thermal events at different temperatures. This fact is most likely due to the presence of water molecules with varying bonding force. For Ca-montmorillonite (Hendricks et al. 1940; Mackenzie 1950; Poinsignon et al. 1982; Guindy et al. 1985; Girgis et al. 1987; Zabat and Van Damme 2000) there is a first dehydration event near 60–90 °C, usually attributed to water loosely bonded, and another event at 110–150 °C, attributed to strongly held water. Guindy et al. (1985) derived dehydration activation energies, although they considered a single dehydration reaction, whereas Poinsignon et al. (1982) and more recently Zabat and Van Damme (2000) derived activation energies for each thermal event, assuming that both are a first-order reaction. Finally, Bray and Redfern (1999) carried out a thorough investigation using isothermal gravimetric analysis to determine both the activation energy and the mechanism of the 2-step dehydration reaction. However, the different thermal analysis techniques provide results that cannot be easily related to structural information from XRD studies, especially at low temperature. The reason is that thermal analysis probes all types of adsorbed water. For example, part of the water quantified by thermal analysis can correspond to interlayer water but also to water molecules located on the external smectite surface and in micro- and macro-pores. In contrast, XRD analysis only probes water located in the interlayer. An additional problem of thermal analysis studies is that interlayer, external and pore water may be lost following a different type of reaction mechanism. Thus, an accurate determination of smectite behavior during dehydration and of dehydration kinetics using XRD focuses on interlayer water and provides fundamental information for the understanding of smectite structural dehydration at the crystal scale.

Material and methods

Sample preparation

The smectite used for this study is the SWy-2 montmorillonite from the Source Clay Repository of The Clay Minerals Society, with a similar structural formula to that determined for SWy-1 by Van Olphen and Fripiat (1979): $[(Al_{3.01}Fe_{0.41}Mn_{0.01}Ti_{0.02}Mg_{0.54})(Si_{7.98}Al_{0.02})O_{20}(OH)_4]M^{+}_{0.55}$, obtained on the <2 µm size fraction. This montmorillonite is originally Na-saturated. The <1 µm size fraction was separated by centrifugation and calcium-exchanged at room temperature with a 1 mol/L $CaCl_2$ solution (1 g of solid per 250 mL of solution). The suspension was shaken mechanically for 24 h, then the solid fraction was separated by centrifugation and a fresh $CaCl_2$ solution was added. The exchange procedure was repeated three times to ensure a complete cation exchange. Removal of the excess salt was performed by washing the solid three times by immersion for 24 h in distilled water with solid-liquid separation performed by centrifugation.

Isothermal X-ray diffraction

The XRD patterns were recorded using an Inel CPS120 detector coupled to a Microsource with an Anton Paar HTTK 10 high temperature stage. This instrument has a curved position-sensitive detector (PSD) spanning 120 °2θ and fixed beam-sample-detector geometry, which enables the simultaneous acquisition of diffraction data at all angles within the detector range. The angle of incidence of the beam on the sample was optimized to improve the quality of the experimental patterns in the 4–40 °2θ region and was set to ~1.5°. A slurry of the Ca-SWy-2 sample was deposited directly on the Pt strip heater of the Anton Paar equipment

and dried at room conditions (~25 °C and 60–65% RH). Immediately after the desired temperature was reached, thirty snapshots, each of 30 seconds duration were recorded isothermally from 30 to 170 °C in 5 °C steps. After a total of ~15 min, an apparent equilibrium was reached where there was almost no further evolution of the sample. An additional isothermal run was performed at 37 °C to better cover the dehydration process of bihydrated layers into mono-hydrated layers. The data acquisition software used with the diffractometer required 2 s to transfer the data to a computer. Therefore, a period of 32 s separated the collection of two consecutive patterns and the reaction time attributed to each pattern was considered as the median time of each individual snapshot. Between each isothermal run, the sample was allowed to cool down to room temperature, and after remaining at this condition for about one hour we verified that no irreversible layer dehydration had occurred during the heating experiment. This was the case below 90 °C. However, for higher temperatures irreversible dehydration occurred and new samples were therefore prepared from fresh slurry for each subsequent isothermal experiment.

X-ray diffraction profile modeling of 00*l* reflections

The PSD geometry differs from that of the classical scanning with the usual Bragg-Brentano geometry for which the XRD profile modeling algorithms have been developed. Indeed, in the PSD geometry, where the angle between incident beam and sample surface remains constant, the diffraction series are produced by different particles, according to their different orientation. In an oriented mount, all flat particles tend to be near-parallel to the sample substrate and the abundance of particles lying at a specific angle to the substrate is expected to decrease as the angle increases. This means that the intensities of the 00*l* peaks are likely to decrease with increasing angle and broaden compared to a pattern from an oriented mount using a scanning X-ray diffractometer. However, because the incident X-ray beam from the Microsource used for this study is much more collimated than that from a classical X-ray tube, this textural effect is reduced and the peaks obtained are narrower and closer to the true Bragg reflection widths. These differences in peak profile character do not challenge the possibility of using profile modeling methods with data from PSD diffractometers as already demonstrated by Wilson et al. (2004). We also discuss this point below using the modeling results.

The experimental XRD profiles of Ca-SWy-2 smectite were modeled using the algorithms developed initially by Sakharov and Drits (1973) and Drits and Sakharov (1976) over the range 4–38 °2θ using a trial-and-error approach. The mass absorption coefficient (μ*) was set to 45 cm^2/g, as recommended by Moore and Reynolds (1997). The z-coordinates for all atoms within the 2:1 layer framework were set as proposed by Moore and Reynolds (1997). The z-coordinates of interlayer species for dehydrated (LT 0W – 9.7 Å) and mono-hydrated (LT 1W – 11.6–12.9 Å) smectite layers were also set as proposed by Moore and Reynolds (1997). However, those for bihydrated (LT 2W – 14.9–15.4 Å) layers were taken from Ferrage et al. (2005b), who found a best fit between experimental and calculated patterns by placing the cation in the centre of the interlayer and one plane of H_2O molecules on both sides of it. The distance along the **c*** axis from the plane containing interlayer cations to the planes containing H_2O molecules is ~1.2 Å. The coherent scattering domain size (CSDS) along the **c*** axis was characterized by setting a maximum value at 70 layers, and a mean CSDS value (N; Drits et al. 1997) which was adjusted. The σ_z parameter accounts for the fluctuations of the layer thickness around a mean value, and its value corresponds to the standard deviation of a Gaussian-type distribution centered on the mean layer thickness value (Guinier 1964; Drits and Tchoubar 1990; Ferrage et al. 2005b). The overall fit quality was assessed using the R_p parameter (Howard and Preston 1989). This unweighted parameter was preferred because it is mainly influenced by misfits in the most intense diffraction maxima such as the 001 reflection, which contains essential information on the proportions of the different layer types and on their respective layer thickness. With increasing dehydration, a gradual increase of R_p values was observed in this study. This variation is likely to be related to the decrease of the structure factor as the amount of interlayer water decreases, which, in turn, decreases the signal:noise ratio and leads to an apparent reduction of the quality of the fit. The signal:noise ratio could have been decreased by smoothing the experimental data but we chose not to apply such treatment to avoid smoothing out any feature in the pattern.

The fitting procedure was described in detail by Ferrage et al. (2005b). Briefly this strategy consists of using a main structure, of one layer type when feasible, to reproduce as much as possible of the experimental XRD pattern. If necessary, additional contributions to the diffracted intensity are introduced to account for the misfit between calculated and experimental patterns. Up to four mixed-layer structures (each with different proportions of layer types) were necessary to reproduce some of the experimental patterns, because of the very heterogeneous structures observed. However, layers with the same hydration state present in the different mixed-layer structures were assumed to have identical parameters (chemical composition, layer thickness, and set of atomic coordinates) to reduce the number of variable parameters. Similarly, identical values of the N and σ_z parameters and water content were used for all mixed-layer structures of a given pattern, although these parameters were allowed to vary as a function of temperature and time (that is, for different patterns). The relative proportions of the different mixed-layer structures and that of the different layer types within them were also variables in the fitting procedure.

RESULTS

Qualitative observation of the evolution of the 001 reflection upon heating

Figure 1 shows the evolution of the position, shape and intensity of the 001 reflection as a function of time for some of the heating temperatures. At 30 °C, the 001 reflection is originally at ~15.45 Å, indicating a bihydrated state. With increasing time, no major evolution is observed in peak shape although there is a slight shift to 15.23 Å. At 37 °C, there are evident modifications of the experimental patterns as time progresses. The 001 peak decreases in intensity, shifts to ~14.23 Å and broadens, developing a tail toward the high-angle side. According to Méring's principle (Méring 1949) this evolution is likely to be related to the presence of interstratified layers with smaller layer thickness. At 45 °C, the 001 reflection first decreases in intensity and then increases and becomes relatively narrow, although slightly asymmetric. The final d_{001} value at ~12.8 Å for this isotherm indicates that the final structure is rather homogeneous with a high amount of 1W layers, although a small amount of bihydrated layers contribute some intensity to the low-angle side of the final 001 peak profile. A similar evolution is observed for the sample recorded at 70 °C, with the difference that at the end of the experiment the peak shape is almost symmetrical and indicates that a homogeneous mono-hydrated state is reached. At 90 and 100 °C, the 001 peak near 12.5 Å decreases in intensity, broadens and becomes asymmetric, with a tail toward the high-angle side. These modifications indicate a second step of dehydration producing the transition from the mono-hydrated state to the dehydrated state.

In all the experiments, a shift in peak position is noticed, which is faster at the beginning of the reaction and then approaches the final value more slowly. The evolution of the $d_{(001)}$ value is plotted as a function of temperature and time in Figure 2a using a 3-dimensional plot and the corresponding projection on the temperature-time plane. From room temperature to 30 °C the sample remains bihydrated, from 30 to 90 °C there is the 2W-1W layer transition, and, finally, the 1W-0W transition is observed for a temperature higher than 90 °C.

This qualitative observation of the experimental XRD patterns shows that the dehydration of Ca-montmorillonite occurs by steps corresponding to discrete 2W, 1W, and then 0W hydration states. In addition, the 001 peak shape indicates that the structure evolves gradually from one hydration state to the other via mixed-layer structures. However, these observations are not sufficient to obtain a thorough understanding of the structure evolution during dehydration or to determine the corresponding kinetic parameters and mechanisms of dehydration. Indeed, the obvious presence of two processes (2W to 1W and 1W to 0W)

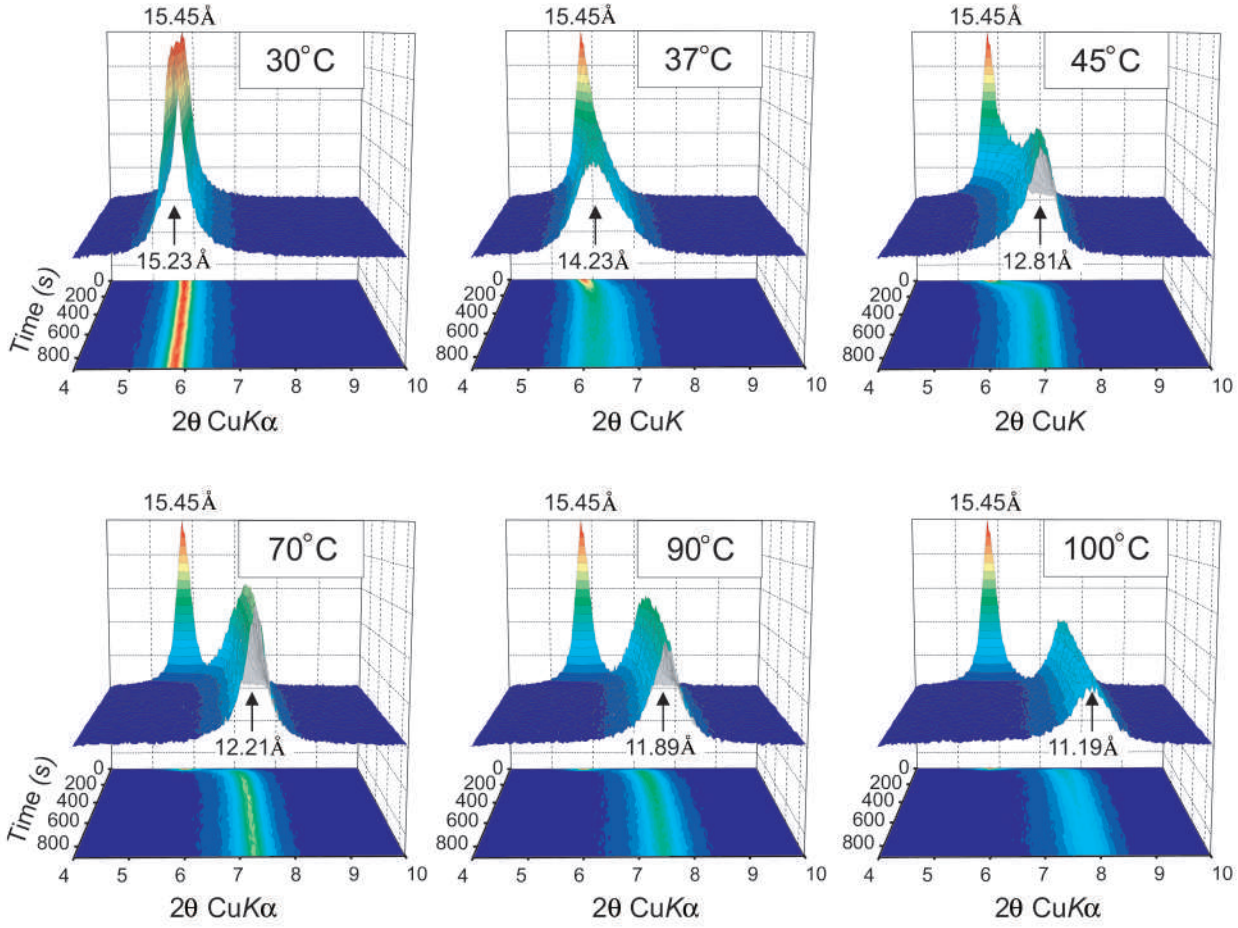

FIGURE 1. Evolution of the smectite 001 reflection as a function of time for different isotherms.

requires their decoupling by a precise quantification of the relative proportion of different layer types. This quantification cannot be carried out by simply using the position of the 001 reflection since this position is determined by the interstratification of layers with contrasting structure factors and with layer thickness that may vary through the time-temperature domain. The modeling of the complete XRD profile is therefore necessary.

Modeling of X-ray diffraction profiles

A total of 630 XRD profiles were modeled in the 30–125 °C range of temperature (30 patterns per isotherm). Uncertainties were estimated for variable parameters that will be used for the kinetic study in the companion paper (relative abundance of 2W, 1W and 0W layers, layers thickness of 1W and 2W layers). For the relative abundance of layers, the uncertainty is higher as the hydration heterogeneity increases. For example, it is easier to detect the presence of a given layer type when its proportion is very high (close to 100%) or very low (close to 0%). Hence the uncertainty on the layer proportion was considered to be ±2% when the abundance of the given layer is 100% or 0% and ±5% when the layer represents 50% of the total layer contribution, with a linear dependence for intermediate values. On the other hand, the uncertainty on the layer thickness is mainly dependent on the abundance of the layer considered, with a better sensitivity where the layer proportion is high. Thus, the uncertainty values increase from ±0.02 to ±0.05 Å, which corresponds to 100% and ~0% of the total layer contribution, respectively.

Calculated and experimental profiles of some selected samples are shown together with their fit residuals in Figure 3a (for the 2W-1W transition) and Figure 3b (for the 1W-0W transition). Figure 4 illustrates the relative contributions from the different mixed-layer structures, for representative XRD patterns. The relative proportions of the three layer types are shown for all the isotherms as a function of time in Figure 5, whereas the abundance of individual layer types are shown in Figures 2b–2d in time-temperature space. Finally, the evolution of the other structural parameters from the calculation (LT 2W, LT 1W, nH_2O σ_z, and N in CSDS) is plotted as a function of temperature and time in Figures 2e–2l.

The 2W-1W transition

The transition from the bihydrated to the mono-hydrated state occurs through very heterogeneous structures with broad 001 reflection (Fig. 3a) and irrational 00*l* series. The initial smectite is modeled with two structures, one containing only 2W layers and a mixed-layer structure containing the three layer types (2W:1W:0W ratio 65:25:10—Fig. 4a). The 2W structure accounts for most of the 001 pattern intensity, whereas the contribution

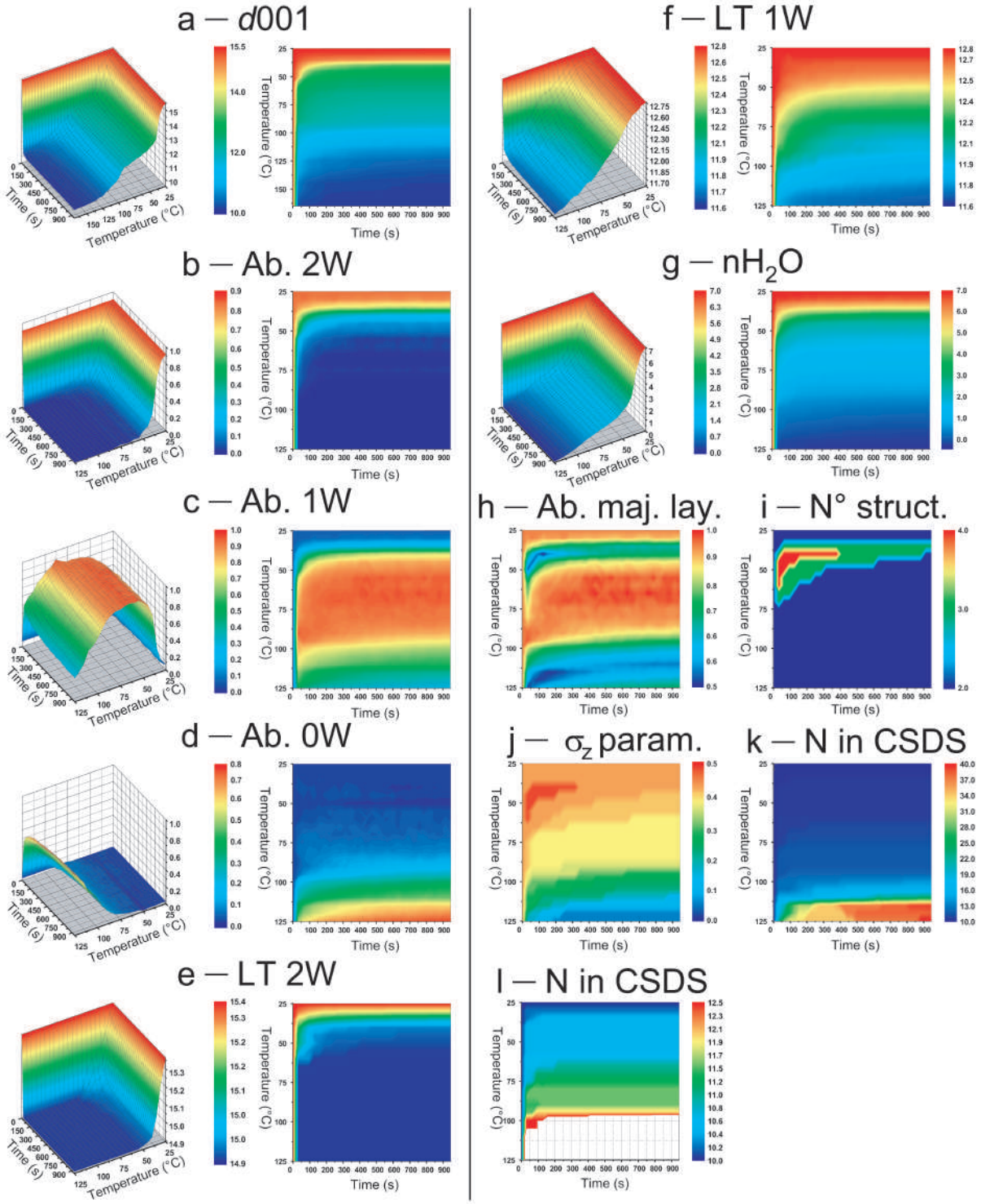

Figure 2. Evolution of various parameters resulting from the XRD modeling during smectite dehydration, in the time-temperature domain. For each of the following parameters, a color-coded 3-D plot and its corresponding projection onto the time-temperature plane are shown: (**a**) 001 reflection position in Å. (**b**) Relative abundance of bihydrated layers. (**c**) Relative abundance of mono-hydrated layers. (**d**) Relative abundance of dehydrated layers. (**e**) Layer thickness of bihydrated layers in Å. (**f**) Layer thickness of mono-hydrated layers in Å. (**g**) Number of water molecules per $O_{20}(OH)_4$. The following parameters are mapped in time-temperature space: (**h**) Relative abundance of the prevailing layer type in percentages. (**i**) Number of discrete structures used during the XRD profile modeling process. (**j**) Layer thickness fluctuation parameter, σ_z, in Å. (**k**) Number of layers in the coherent scattering domain. (**l**) Enlarged view of figure (**k**) for the first dehydration stages.

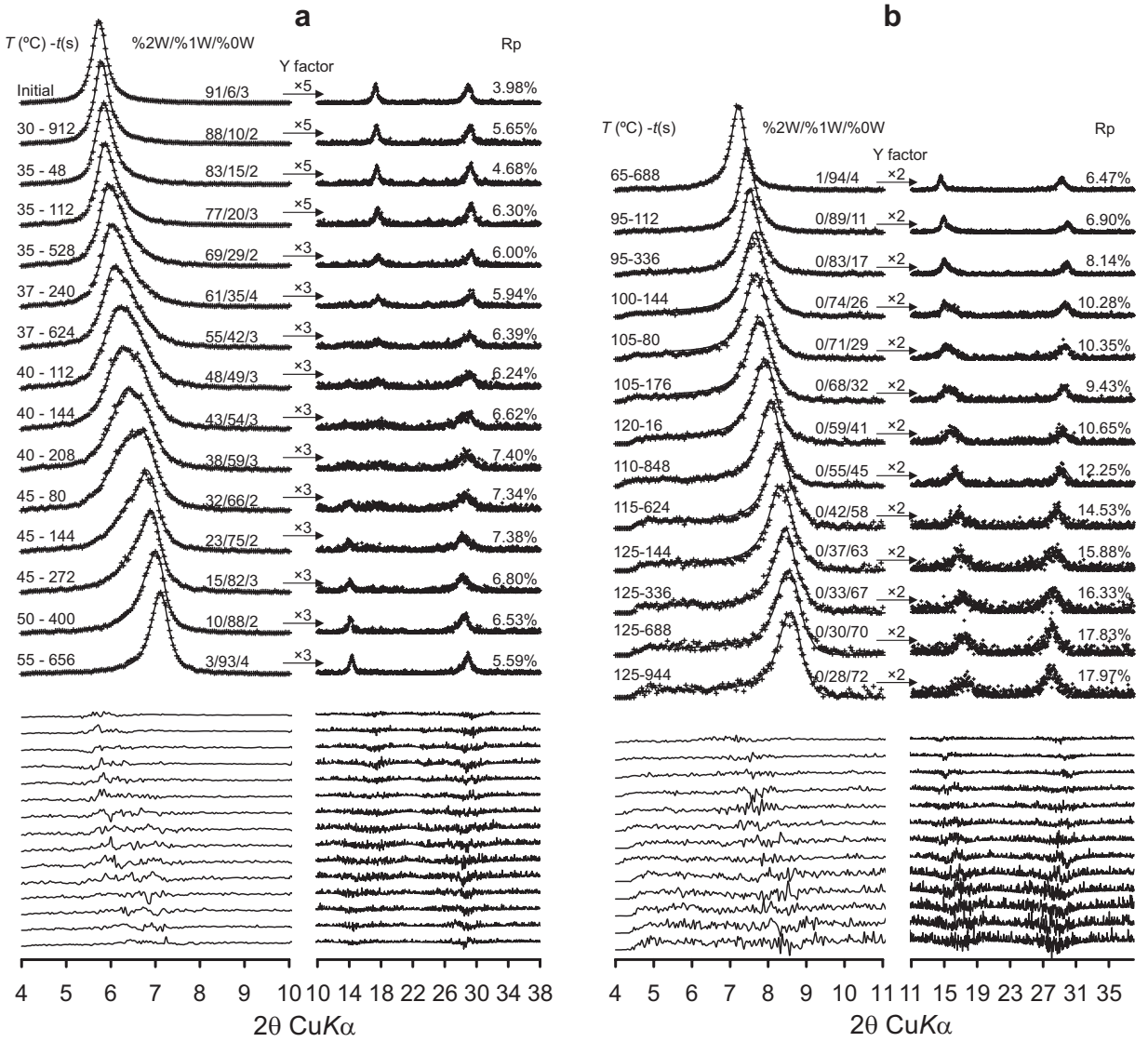

FIGURE 3. Comparison between experimental (cross symbols) and calculated (lines) XRD patterns as a function of time (t) and temperature (T) for some selected patterns. Difference plots are shown at the bottom of the figure. The relative abundance of bi-, mono-hydrated and dehydrated layers, as well as the goodness of fit (R_p), are indicated for each pattern. Arrows indicate a modified scale factor for the high-angle region. (**a**) Characteristic patterns of the transition from the bi- to the mono-hydrated state. (**b**) Characteristic patterns of the transition from the mono-hydrated to dehydrated state.

from the mixed-layer structure allows reproducing the asymmetry on the high-angle side of the 001 peak and on the low-angle side of the third peak (005). With increasing dehydration, the 001 peak asymmetry increases and is reproduced by introducing additional 1W layers in the two contributing structures at the expense of 2W layers. However, there is a point along the dehydration process at which two structures are not sufficient to reproduce correctly the experimental pattern. At 35 °C, it is necessary to split the main structure into two mixed-layer structures with different proportions of 2W and 1W layers (Fig. 4b). With increasing dehydration, the 2W layer proportion in these two contributions decreases. For some patterns the appearance of an additional peak at ~14 °2θ corresponding to the 002 reflection of a mono-hydrated structure, required a fourth mixed-layer structure, with a 2W:1W ratio 15:85, to be included (Fig. 4c). As dehydration progresses (45 °C), the number of structures necessary for the fit decreases first to three (Fig. 4d) and then to two (Fig. 4e), as the relative overall proportion of 1W layers increases.

The 1W-0W transition

This transition appears to be more homogeneous, with a narrower 001 reflection that gradually shifts toward higher angles (Fig. 3b). However, the irrational (00l) series indicates the presence of 1W and 0W layers in variable amounts. Only two contributing structures were needed to fit the obtained experimental profiles. For the pattern shown in Figure 4f, the first contribution

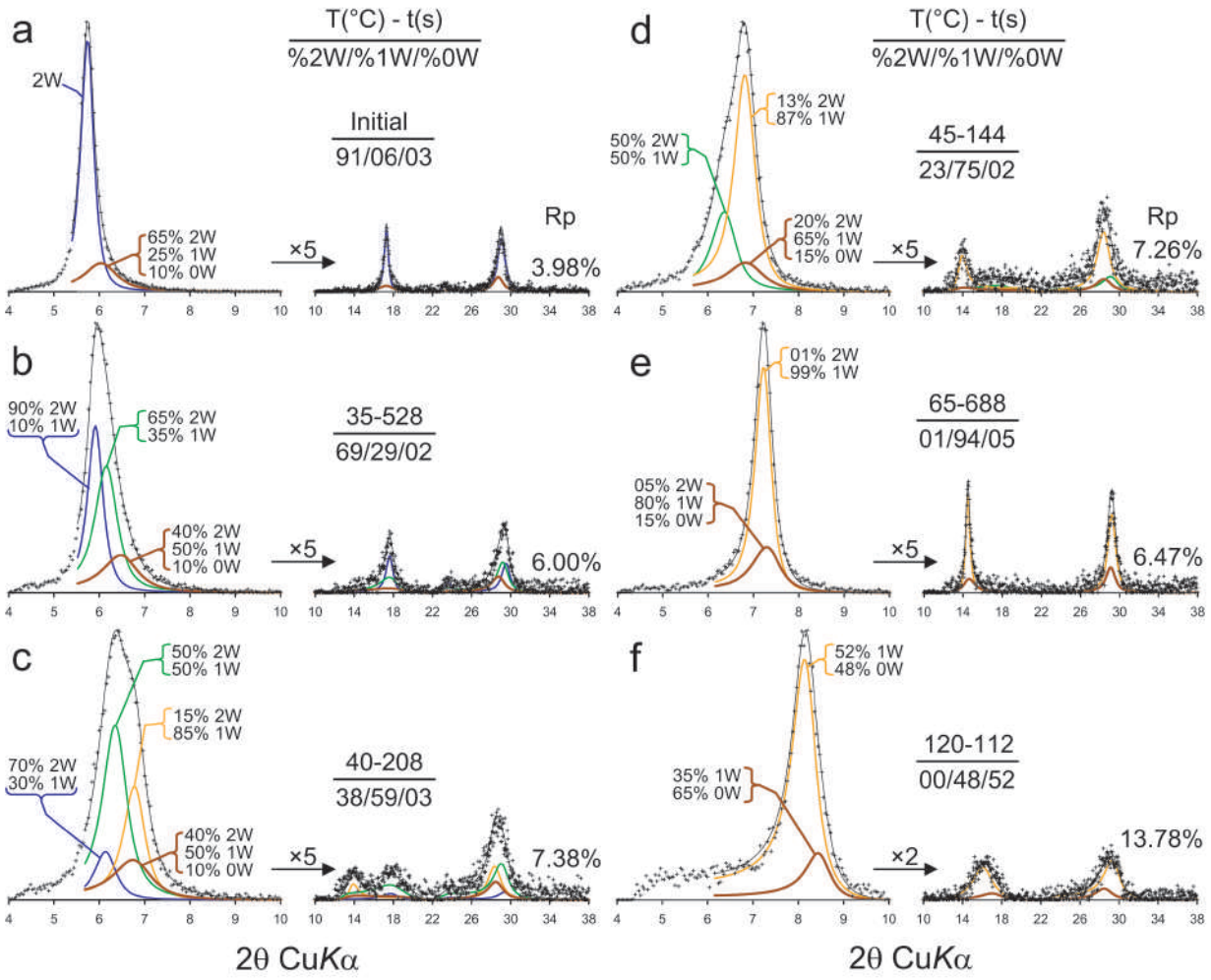

FIGURE 4. Respective contributions of the various mixed-layer structures to the calculated profiles for selected XRD patterns. Arrows indicate a modified scale factor for the high-angle region. The experimental and calculated XRD patterns are shown as crosses and as solid lines, respectively. The contribution of the different mixed-layer structures to the calculated patterns are shown as blue, green, orange, and brown lines. The temperature, time, and overall proportion of layers (2W, 1W, 0W) at these conditions and the proportion of layers in each mixed-layer structure used for the modeling are indicated. (**a**) Initial sample. (**b**) 35 °C; 528 s. (**c**) 40 °C; 208 s. (**d**) 45 °C; 144 s. (**e**) 65 °C; 688 s. (**f**) 120 °C; 112 s.

incorporates 1W and 0W layers in similar proportions whereas 0W layers are predominant in the second structure. Both the proportion of this second structure and its relative amount of 0W layers increase with increasing dehydration.

DISCUSSION

Application of X-ray diffraction profile modeling method to XRD-PSD data

For all the isotherms performed, the evolution of the smectite-water structure was first very rapid and then slowed down as it approached an almost stable state after about 16 m. This rapid transformation requires the use of a fast XRD data acquisition method to obtain sufficiently resolved results. The use of XRD-PSD is thus particularly suited for this type of study, although a synchrotron source could lead to an even better resolution. However, one may question the validity of trying to reproduce experimental patterns obtained using a curved PSD system with a modeling algorithm that was developed for scanning diffractometers. As indicated in the methods section, the difference in instrumental geometry induces some minor differences in the experimental patterns. The diffractometer with a Microsource X-ray source and a curved PSD produces narrower 00*l* peaks and a very small decrease of their intensity and broadening with increasing diffraction angle. Such narrowing of 00*l* reflections, due to the very small divergence of the incident beam, produces a slight increase of the size of CSD calculated from the profile. The analysis of a similar Ca-montmorillonite (SWy-1; Ferrage et al. 2005b) produced a coherent scattering domain of 6–8 layers in a traditional scanning system, and of 10 layers in the present study. In addition, the slight broadening with increasing angle is induced by the fact that, in this system, the diffracted intensity for each angle results from different particles, because the beam-sample incidence angle is fixed (Wilson et al. 2004). This effect, which is very small when comparing qualitatively two patterns

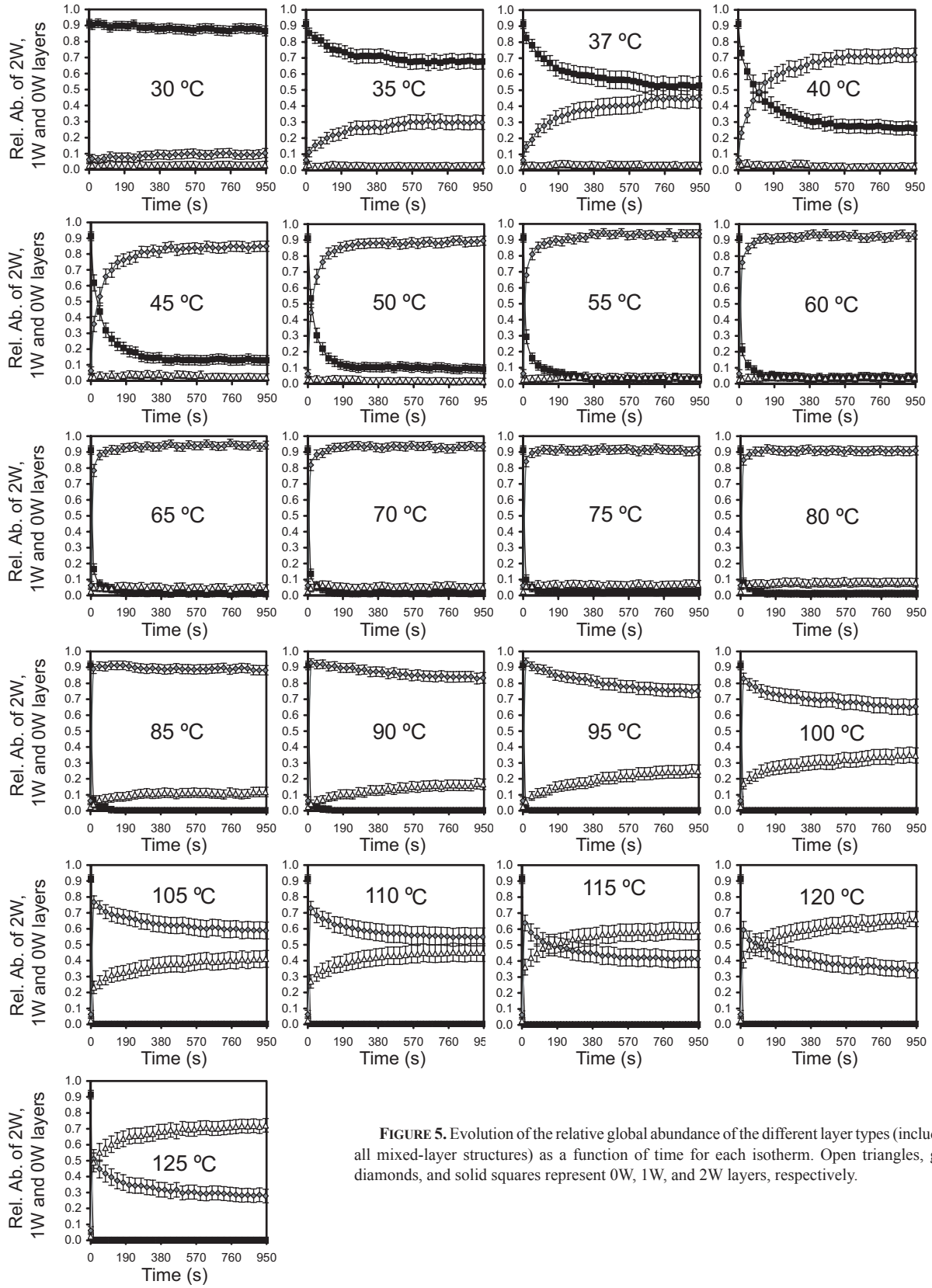

FIGURE 5. Evolution of the relative global abundance of the different layer types (including all mixed-layer structures) as a function of time for each isotherm. Open triangles, gray diamonds, and solid squares represent 0W, 1W, and 2W layers, respectively.

recorded on static (PSD) and scanning diffractometers, is likely to be taken into account during the modeling by increasing the value of σ_z. Indeed, this parameter simulates crystal strain and has a similar effect on the calculated profile (Guinier 1964; Drits and Tchoubar 1990; Ferrage et al. 2005b). The σ_z value obtained for the starting sample is 0.40 Å, not very different from that of 0.30 Å determined by Ferrage et al. (2005b) with a scanning diffractometer. In addition, σ_z decreases to 0.05 Å for the most dehydrated sample. If we consider that the broadening for this latter sample is only due to the experimental set-up, such a low σ_z value indicates a negligible broadening effect caused by the curved PSD on the σ_z values obtained in the present study. Therefore, in spite of the different geometry, the difference in the values of structural parameters resulting from XRD profile modeling of PSD data is very small and the variation of these parameters through the dehydration process are not significantly affected by the instrumental set-up.

Evolution of the smectite-water structure as a function of dehydration

Evolution of layer proportion

The qualitative observation of the experimental patterns in the temperature-time space reveals the presence of some domains with an almost homogeneous hydration state, and other domains in which the structure was very heterogeneous (Figs. 1 and 2a). Quantification of the different types of layers (2W, 1W, and 0W) as a function of time for each isotherm can be used to analyze further the above observations (Figs. 2b–2d and 5). At 30 °C, the great majority of layers remain in a 2W state. For higher temperatures (between 35 and 50 °C), we observe the almost complete transition from 2W to 1W layers. During this transition the relative amount of dehydrated layers is systematically low (<3%). These layers could be related to the presence of some non-expandable illitic layers as determined from ethylene-glycol treatment by Ferrage et al. (2005b). In such low proportion and because of the small structure factor of 0W layers, it is very difficult to discriminate between a layer thickness of 9.98 Å typical of illite layers and that of 9.7 Å, and no attempt was made to differentiate between them. Between 55 and 85 °C, 1W layers prevail (Fig. 5), as indicated also in Figure 2a. However, over this range of temperature, the proportion of 0W layers increases slightly at the expense of 1W layers. Finally, the 1W-0W transition starts above 85 °C but is still not complete at 125 °C (Fig. 5). The second transition (1W-0W) does not begin until the first transition (2W-1W) is complete, indicating that the system evolves in its totality from one hydration state to the other. In addition note that the two transitions occur via mixed-layer structures that transform rapidly during the first stages of each isotherm and then evolve more slowly toward the final state. One may assume that the transition from one hydration state to the other occurs as an energy barrier is surpassed. In this case, the hydration heterogeneity observed at the end of the isothermal experiments and the fact that there is little evolution after a certain time period at each temperature implies the presence of gradual sets of energetic barriers. Recent results obtained from Monte-Carlo simulations by Tambach et al. (2006) support the presence of a wide free-energy barrier for the transition from one hydration state to the other. The possible statistical distribution of water content that may lead some interlayers to have a slightly different hydration state (or different water content) could be one of the causes of the transition of hydrated layers at different temperatures.

It was mentioned above that a complete reversibility of the experiments in a time-scale of about one hour was observed up to 90 °C, allowing the same sample to be used for all isotherms performed below this temperature. It is at about this temperature that the 1W-0W transition starts. Finally, the results from XRD profile modeling show that for temperatures above 105–110 °C, the shape of the plot of the proportion of layers seems to be cut off at low times of reaction. This phenomenon is induced by the rapidly applied high temperature that causes the sample to react before reaching the temperature of the isotherm.

Evolution of crystal parameters

The degree of hydration heterogeneity can be assessed from the modeling results by observing the relative abundance of the prevailing layer type as a function of temperature and time (Fig. 2h). Ferrage et al. (2005b) showed that there is certain correlation between the proportion of the prevailing layer type and the irrational character of the 00*l* series. In the present study we analyze the possible relation between the apparent layer hydration heterogeneity and the evolution of other crystal parameters.

The σ_z parameter, which characterizes the fluctuation in layer thickness (within each layer type: 2W, 1W, and 0W) shows strong modifications with dehydration, from 0.4 Å in the original state to 0.05 Å at the end of the 125 °C isotherm (Fig. 2j). This variation means that any specific layer has an almost constant thickness as its water content decreases. In 2W layers, the electrostatic interaction between layers and cations are weaker, and, possibly the water molecules are non-uniformly distributed, resulting in less parallel layers and higher σ_z values. As dehydration proceeds the interlayer thickness is better constrained by the increasingly higher interaction between cations and the 2:1 layers because of the smaller amount of interlayer water. In addition, σ_z increases locally between 40 and 60 °C for short reaction times (<300 s; Fig. 2j). This temperature-time domain corresponds to a very heterogeneous region of the 2W-1W transition. A similar σ_z increase was also observed by Ferrage et al. (2005b) on the same smectite when the relative humidity was decreased. They attributed this σ_z increase to the incomplete transition of a given interlayer from one hydration state to the next, with the coexistence, within a given interlayer, of different hydration states and interlayer thickness. In the present study, the 2W-1W transition showed a σ_z increase, but not so the 1W-0W transition. In addition, the heterogeneous 2W-1W transition region also needed the highest number of elementary structures for the modeling (Fig. 2i). A similar hypothesis to that of Ferrage et al. (2005b) can be assumed for the observed increase of σ_z values during the 2W-1W transition. The increase of the σ_z parameter values may possibly reflect the layer thickness fluctuation introduced (within a given interlayer) when an incomplete transition between two hydration states occurs. Also, the numerous contributions used to fit the experimental pattern could possibly be related to this increased heterogeneity. For the 1W-0W transition, this phenomenon is not observed, probably because of the smaller number of water molecules implicated, which induce a more

homogeneous transition toward the dehydrated state.

The CSD size along the **c*** axis is rather stable where the 2W and 1W layers prevail, whereas there is a dramatic increase during the 1W-0W transition and where dehydrated layers prevail (Figs. 2k–2l). Note however that during the first step of dehydration the N value is slightly smaller when 2W layers prevail. This phenomenon, already observed as a function of relative humidity (Ferrage et al. 2005b, 2007), may be related to a possible disruption of some 2W layer stacks because of (1) the large amount of water and osmotic swelling induce weaker electrostatic interactions between layers and/or (2) the interstratification of some tri-hydrated layers (3W; Sato et al. 1992). The large N increase in the 1W-0W transition was never found for dehydration occurring as a function of RH by Ferrage et al. (2005b, 2007), although these authors never obtained a Ca-exchanged smectite structure in which dehydrated layers prevailed. Such an increase of the size of the CSD at high temperature may be related to the observed σ_z decrease. Indeed, as layers become more parallel with progressing dehydration more layers can stack in well-ordered sequences along the **c*** axis.

Layer thickness and interlayer water

During dehydration, 2W and 1W layers experience a decrease of layer thickness (Figs. 2e and 2f). This observation is in agreement with results obtained by Ferrage (2004) and Ferrage et al. (2005a, 2005b, 2007), whereas a constant layer thickness has been generally assumed for 00*l* XRD profile modeling in the past (Moore and Reynolds 1997). A reduction of water content is also noticed between ~3.5 and ~0.3 $H_2O/O_{20}(OH)_4$ for 1W and between ~7.4 and ~5.2 $H_2O/O_{20}(OH)_4$ for 2W layers (Fig. 6a). This is responsible for the water content decrease between 60 and 80 °C, where only 1W layers are present in the structure (Fig. 2g). During the 2W-1W layer transition, the amount of interlayer water in 2W layers (before the transition to 1W) decreases. This phenomenon is possibly related to a different organization of the water framework within the interlayer (Rinnert et al. 2005). It could be responsible for the observed hydration heterogeneity and the need of different temperature/energy to produce the change of hydration state. For the mono-hydrated layers a gradual decrease of layer thickness is observed throughout the dehydration process (Fig. 6a).

Although the water content is best quantified using water vapor adsorption-desorption experiments (Bérend et al. 1995, Cases et al. 1992, 1997; Michot et al. 2005), it is possible to determine from our results that a water content of ~1.15 $H_2O/O_{20}(OH)_4$ can be considered as the value below which the 1W-0W transition takes place. The structural formula contains 0.275 Ca atoms per $O_{20}(OH)_4$ and thus, for 1W layers, the limit of water content below which the 1W-0W transition takes place represents ~4.2 water molecules per cation. This value is similar to the 4 molecules of water per Ca atom determined for mono-hydrated Ca-vermiculite by de la Calle et al. (1985) and Rausell-Colom et al. (1980). Rausell-Colom et al. (1980) determined that, in this configuration, the water molecules are strongly linked to the cation with a coordination geometry similar to a very flat tetrahedron. It can be therefore assumed that the 1W-0W transition starts when this configuration is disrupted by the removal of a water molecule. Rausell-Colom et al. (1980) also described 1W layers with only 3 molecules of water per cation when Sr is the interlayer cation. In the present study, the water content decreases down to 2 or 1 water molecules per cation. These low values were not observed by the above authors although they focused on structures having almost 100% of 1W layers. In the present study, 1W layers with <3 water molecules per cation are present when the proportion of 1W layers is below 50% and the structure is therefore very heterogeneous. For water contents higher than 4 molecules per cation it may be assumed that the water molecules are linked to the interlayer cation in a different coordination. Indeed Rausell-Colom et al. (1980) showed a configuration with six H_2O molecules for Ba-vermiculite. A similar configuration could be expected for Ca atoms although the smaller radius of Ca may favor the rapid reorganization in 4-coordination. For water contents higher than 8 water molecules per cation or 2.25 $H_2O/O_{20}(OH)_4$, which corresponds to ~80% 1W layers at the end of the 2W-1W transition (Fig. 6a), it may be assumed that additional water molecules are present. These additional water molecules are easily removed at the end of the 2W-1W transition and may correspond to water that is not coordinated, or weakly so, to the interlayer cation.

For 2W layers, the amount of H_2O molecules per cation determined for our sample is extremely high (19–27 H_2O molecules/Ca atom). Some studies of the water configuration of water in bihydrated states of Ca-vermiculite usually give lower values as determined by Slade et al. (1985; 8.02 H_2O/Ca), de la Calle et al. (1977; 8.60 H_2O/Ca), and Le Renard and Mamy (1971; 4.28 H_2O/Ca) from XRD. However, these values are obtained for vermiculite, which has a high layer charge and thus high Ca content. When recalculating the corresponding values of number of water molecules per unit cell we obtain 7.5, 6.6, and 7.6 $H_2O/O_{20}(OH)_4$, respectively, values that are in agreement with those found in the present study when 2W layers prevail at a level of 70% or more. This comparison may indicate that for low-charge smectite most water molecules in the bihydrated state are not coordinated to the interlayer cation. It can therefore be assumed that in 2W smectite the interlayer cation and its hydration shell control the interlayer aperture, which is then filled by additional water molecules. In this case, increasing the interlayer cation amount may modify the organization of water inside the interlayer. This assumption is confirmed by recent results obtained by Ferrage et al. (2005a). Indeed these authors found a similar interlayer configuration of water molecules distributed around two main positions along the **c*** axis for various smectite samples. With increasing layer charge and thus of the interlayer cation content, they observed a narrower distribution of water molecules around these two main positions, indicating a more structured water framework. This hypothesis is also supported by infrared data (Rinnert et al. 2005).

Figure 6b shows the evolution of layer thickness as a function of percentage of 2W and 1W layers. As determined for water content, it is possible to derive that a layer thickness of ~12 Å represents the value at which the 1W-0W transition starts. In addition it can be noted that as %1W increases there is a very small variation of 1W layer thickness (from 12.75 to 12.60 Å), whereas the layer-thickness variation is larger as %1W decreases again (from 12.00 to 11.65 Å – Fig. 6b). This phenomenon is more obvious when plotting the evolution of layer thickness as

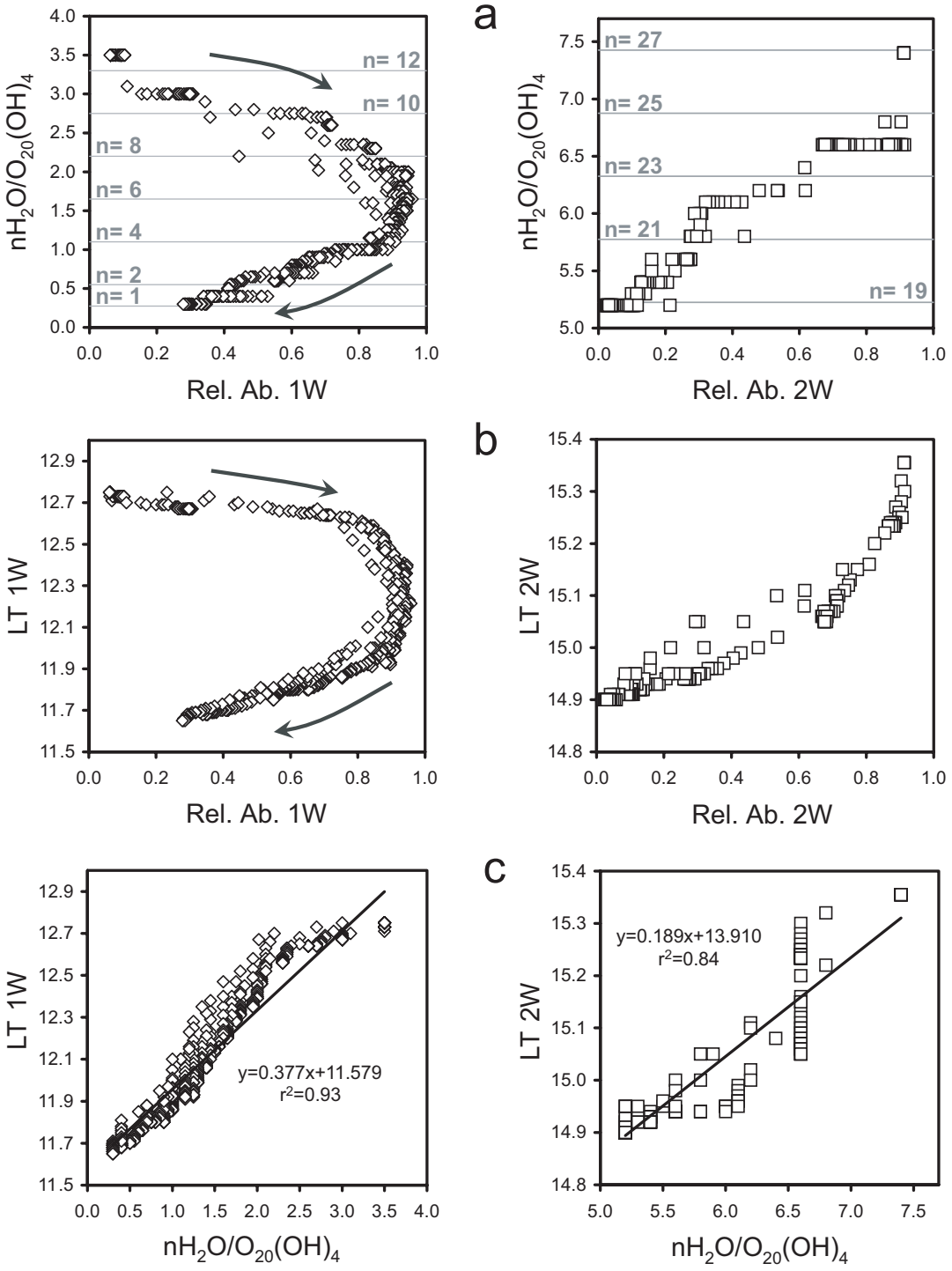

FIGURE 6. Evolution of the layer thickness (LT in Å) and water content for mono-(1W) and bihydrated (2W) layers. (**a**) Evolution of water content as a function of the layer relative abundance. The number n of water molecules per cation is indicated in gray. (**b**) Evolution of layer thickness as a function of the layer relative abundance. (**c**) Evolution of layer thickness as a function of structural water content.

a function of water content (Fig. 6c). The sigmoid shape may indicate three discrete types of structural evolutions during dehydration. Starting from the more hydrated layers, the first step [LT 1W = 12.75–12.65 Å and nH_2O = 3.50–2.10 $H_2O/O_{20}(OH)_4$] shows a limited decrease of layer thickness indicating that the water molecules removed have only a limited effect of the layer thickness and may correspond to the additional water molecules described above that are not coordinated to the interlayer cation. Water and layer thickness reduction during the second and intermediate region [LT 1W = 12.65–12.00 Å and nH_2O = 2.10–1.15

$H_2O/O_{20}(OH)_4$] could possibly correspond to water interacting slightly with the interlayer cation and forming a distant hydration shell, whereas the last region of the graph [LT 1W < 12.00 Å and $nH_2O < 1.15$ $H_2O/O_{20}(OH)_4$] may correspond to the removal of water molecules forming the first hydration shell of the interlayer cation as described above. Because of the fewer data obtained for 2W layers, the shape of the evolution is more difficult to define. Additional spectroscopic data may be necessary to examine the possible different interactions of these water molecules for both 1W and 2W layers. Indeed Rinnert et al. (2005) coupled several spectroscopic and numerical methods and showed that the evolution of the *d*-spacing was not strictly proportional to the amount of interlayer water. These authors interpreted this phenomenon as a different organization of the water molecules within the interlayer of smectite. If the data points in this study are approached by a simple linear regression the slope of the 2W line is twice that of the 1W line. This is likely to be due to the 1W layer having a single plane of water molecules and the 2W layers two planes. For the latter, the influence of the addition or removal of one water molecule on the layer thickness is roughly half of that for 1W layers. This relation has been already observed in dehydration experiments of a Na-saturated saponite using the same type of XRD modeling analysis (Ferrage 2004). Note that although this relation averages the possible different phenomena occurring during the dehydration process (described above for the 1W layers), it allows an approximation of the amount of water molecules for a given layer thickness, a value that will be used in the second part of this study.

Temperature- vs. RH-driven dehydration and global path of smectite dehydration

This study shows that dehydration is a complex process at the crystal scale that involves constant reorganization of water within the interlayer of smectite. Such reorganization is accompanied by the coexistence of layers having different hydration states and a systematic gradual decrease of the layer thickness of structures with any given hydration state. From many points of view, this dehydration is similar to that observed as a function of relative humidity by Ferrage et al. (2005b) on the same smectite SWy-2 sample and using the same XRD profile modeling approach. In both cases there are stable heterogeneous hydration states that do not evolve with time. The data obtained in the present study also indicate that the entire system (layer thickness and hydration state) is governed by local organization of water molecules which can be coordinated, or not, to the interlayer cation. Because the variation of the different structural parameters are similar to those observed by Ferrage (2004) with decreasing RH it should be considered that the global path of smectite dehydration is similar whatever the type of experiment (constant temperature and varying RH or constant RH and varying temperature). The large set of data obtained here can thus be used to build up a precise kinetic model of the dehydration process, as presented in Part 2 of this paper.

Acknowledgments

This study was funded by a Marie-Curie Intra-European fellowship granted to E.F. (contract: MEIF-CT-2004-515386). The manuscript was much improved by the constructive reviews of Bruno Lanson, Laurent Michot, and an anonymous reviewer. The editorial assistance of AE Warren Huff is acknowledged.

References cited

Bérend, I., Cases, J.M., François, M., Uriot, J.P., Michot, L.J., Masion, A., and Thomas, F. (1995) Mechanism of adsorption and desorption of water vapour by homoionic montmorillonites: 2. The Li^+, Na^+, K^+, Rb^+ and Cs^+ exchanged forms. Clays and Clay Minerals, 43, 324–336.

Bradley, W.F., Grim, R.E., and Clark, G.F. (1937) A study of the behavior of montmorillonite upon wetting. Zeitschrift Kristallographie, 97, 216–222.

Bray, H.J. and Redfern, S.A.T. (1999) Kinetics of dehydration of Ca-montmorillonite. Physics and Chemistry of Minerals, 26, 591–600.

Bray, H.J., Redfern, S.A.T., and Clark, S.M. (1998) The kinetics of dehydration in Ca-montmorillonite: an in situ X-ray diffraction study. Mineralogical Magazine, 62, 647–656.

Calarge, L., Lanson, B., Meunier, A., and Formoso, M.L. (2003) The smectitic minerals in a bentonite deposit from Melo (Uruguay). Clay Minerals, 38, 25–34.

de la Calle, C., Pezerat, H., and Gasperin, M. (1977) Poblèmes d'ordre-désordre dans les vermiculites—Structure du minéral calcique hydraté à deux couches. Journal de physique, 38, C7 128–133.

de la Calle, C., Suquet, H., and Pezerat, H. (1985) Vermiculites hydratées à une couche. Clay Minerals, 20, 221–230.

Cases, J.M., Bérend, I., Besson, G., François, M., Uriot, J.P., Thomas, F., and Poirier, J.P. (1992) Mechanism of adsorption-desorption of water vapor by homoionic montmorillonite. 1. The sodium exchanged form. Langmuir, 8, 2730–2739.

Cases, J.M., Bérend, I., François, M., Uriot, J.P., Michot, L.J., and Thomas, F. (1997) Mechanism of adsorption and desorption of water vapour by homoionic montmorillonite: 3. the Mg^{2+}, Ca^{2+}, Sr^{2+} and Ba^{2+} exchanged forms. Clays and Clay Minerals, 45, 8–22.

Cuadros, J. (1997) Interlayer cation effects on the hydration state of smectite. American Journal of Science, 297, 829–841.

Drits, V.A. and Sakharov, B.A. (1976) X-Ray structure analysis of mixed-layer minerals, 256 p. Doklady Akademii nauk SSSR, Moscow.

Drits, V.A. and Tchoubar, C. (1990) X-ray diffraction by disordered lamellar structures: Theory and applications to microdivided silicates and carbons, 371 p. Springer-Verlag, Berlin.

Drits, V.A., Srodon, J., and Eberl, D.D. (1997) XRD measurement of mean crystallite thickness of illite and illite/smectite: reappraisal of the kubler index and the scherrer equation. Clays and Clay Minerals, 45, 461–475.

Ferrage, E. (2004) Etude expérimentale de l'hydratation des smectites par modélisation des raies 00*l* de diffraction des rayons X-Implications pour l'étude d'une perturbation thermique sur la minéralogie de l'argilite du site Meuse-Haute Marne. Environnemental and Geochimistry Group, p. 326. Université Joseph Fourrier, Grenoble.

Ferrage, E., Lanson, B., Malikova, N., Plançon, A., Sakharov, B.A., and Drits, V.A. (2005a) New insights on the distribution of interlayer water in bi-hydrated smectite from X-ray diffraction profile modeling of 00*l* reflections. Chemistry of Materials, 17, 3499–3512.

Ferrage, E., Lanson, B., Sakharov, B.A., and Drits, V.A. (2005b) Investigation of smectite hydration properties by modeling of X-ray diffraction profiles. Part 1. Montmorillonite hydration properties. American Mineralogist, 90, 1358–1374.

Ferrage, E., Lanson, B., Sakharov, B.A., Jacquot, E., Geoffroy, N., and Drits, V.A. (2007) Investigation of smectite hydration properties by modeling of X-ray diffraction profiles. Part 2. Influence of layer charge and charge location. American Mineralogist, 92, in press.

Girgis, B.S., El-Barawy, K.A., and Felix, N.S. (1987) Dehydration kinetics of some smectites: a thermogravimetric study. Thermochimica Acta, 111, 9–19.

Glaeser, R. and Méring, J. (1968) Domaines d'hydratation des smectites. Comptes-Rendus de l'Académie des Sciences de Paris, 267, 463–466.

Glaeser, R., Mantine, I., and Méring, J. (1967) Observations sur la beidellite. Bulletin du Groupe Français des Argiles, 19, 125–130.

Guindy, N.M., El-Akkad, T.M., Flex, N.S., El-Massry, S.R., and Nashed, S. (1985) Thermal dehydration of mono- and di-valent montmorillonite cationic derivates. Thermochimica Acta, 88, 369–378.

Guinier, A. (1964) Théorie et technique de la radiocristallographie, 740 p. Dunod, Paris.

Harward, M.E. and Brindley, G.W. (1965) Swelling properties of synthetic smectites in relation to lattice substitutions. Clays and Clay Minerals, 13, 209–222.

Harward, M.E., Carstea, D.D., and Sayegh, A.H. (1969) Properties of vermiculites and smectites: expansion and collapse. Clays and Clay Minerals, 16, 437–447.

Hendricks, S.B., Nelson, R.A., and Alexander, L.T. (1940) Hydration mechanism of the clay mineral montmorillonite saturated with various cations. Journal of American Chemical Society, 62, 1457–1464.

Howard, S.A. and Preston, K.D. (1989) Profile fitting of powder diffraction patterns. In D.L. Bish and J.E. Post, Eds., Modern Powder Diffraction, 20, p. 217–275. Reviews in Mineralogy, Mineralogical Society of America, Chantilly, Virginia.

Iwasaki, T. and Watanabe, T. (1988) Distribution of Ca and Na ions in dioctahedral smectites and interstratified dioctahedral mica/smectites. Clays and Clay

Minerals, 36, 73–82.
Kittrick, J.A. (1969a) Interlayer forces in montmorillonite and vermiculite. Soil Science Society of America Journal, 33, 217–222.
——— (1969b) Quantitative evaluation of the strong-force model for expansion and contraction of vermiculite. Soil Science Society of America Journal, 33, 222–225.
Laird, D.A. (1996) Model for crystalline swelling of 2:1 phyllosilicates. Clays and Clay Minerals, 44, 553–559.
——— (1999) Layer charge influences on the hydration of expandable 2:1 phyllosilicates. Clays and Clay Minerals, 47, 630–636.
Laureiro, Y., Jerez, A., Rouquerol, F., and Rouquerol, J. (1996) Dehydration kinetics of Wyoming montmorillonite studied by controlled transformation rate thermal analysis. Thermochimica Acta, 278, 165–173.
Le Renard, J. and Mamy, J. (1971) Etude de la structure des phases hydratées des phlogopites altérées par des projections de fourier monodimensionnelles. Bulletin du Groupe Français des Argiles, 23, 119–127.
Mackenzie, R.C. (1950) Some notes on the hydration of montmorillonite. Clay Mineral Bulletin, 1, 115–119.
——— (1952) Discussion on irreversible dehydration in montmorillonite. Clay Mineral Bulletin, 1, 226–227.
Méring, J. (1949) L'interférence des rayons-X dans les systèmes à stratification désordonnée. Acta Crystallographica, 2, 371–377.
Méring, J. and Glaeser, R. (1954) Sur le rôle de la valence des cations échangeables dans la montmorillonite. Bulletin de la Société Francaise de Minéralogie et Cristallographie, 77, 519–530.
Michot, L.J., Bihannic, I., Pelletier, M., Rinnert, E., and Robert, J.L. (2005) Hydration and swelling of synthetic Na-saponites: influence of layer charge. American Mineralogist, 90, 166–172.
Mooney, R.W., Keenan, A.G., and Wood, L.A. (1952) Adsorption of water by montmorillonite. II. Effect of exchangeable ions and lattice swelling as measured by X-ray diffraction. Journal of American Chemical Society, 74, 1371–1374.
Moore, D.M. and Hower, J. (1986) Ordered interstratification of dehydrated and hydrated Na-smectite. Clays and Clay Minerals, 34, 379–384.
Moore, D.M. and Reynolds, R.C., Jr (1997) X-ray Diffraction and the Identification and Analysis of Clay Minerals, 322 p. Oxford University Press, New York.
Nagelschmidt, G. (1936) On the lattice shrinkage and structure of montmorillonite. Zeitschrift Kristallographie, 93, 481–487.
Norrish, K. (1954) The swelling of montmorillonite. Discussions of the Faraday society, 18, 120–133.
Poinsignon, C., Yvon, J., and Mercier, R. (1982) Dehydration energy of the exchangeable cations in montmorillonite. A DTA study. Israel Journal of Chemistry, 22, 253–255.
Rausell-Colom, J.A., Fernandez, M., Serratosa, J.M., Alcover, J.F., and Gatineau, L. (1980) Organisation de l'espace interlamellaire dans les vermiculites monocouches et anhydres. Clay Minerals, 15, 37–58.
Rinnert, E., Carteret, C., Humbert, B., Fragneto-Cusani, G., Ramsay, J.D.F., Delville, A., Robert, J.L., Bihannic, I., Pelletier, M., and Michot, L.J. (2005) Hydration of a synthetic clay with tetrahedral charges: a multidisciplinary experimental and numerical study. Journal of Physical Chemistry B, 109, 23745–23759.
Sakharov, B.A. and Drits, V.A. (1973) Mixed-layer kaolinte-montmorillonite: a comparison observed and calculated diffraction patterns. Clays and Clay Minerals, 21, 15–17.
Sato, T., Watanabe, T., and Otsuka, R. (1992) Effects of layer charge, charge location, and energy change on expansion properties of dioctahedral smectites. Clays and Clay Minerals, 40, 103–113.
Sato, T., Murakami, T., and Watanabe, T. (1996) Change in layer charge of smectites and smectite layers in illite/smectite during diagenetic alteration. Clays and Clay Minerals, 44, 460–469.
Slade, P.G., Stone, P.A., and Radoslovitch, E.W. (1985) Interlayer structures of the two-layer hydrates of Na- and Ca-vermiculites. Clays and Clay Minerals, 33, 51–61.
Tambach, T.J., Bolhuis, P.G., Hensen, E.J.M., and Smit, B. (2006) Hysteresis in clay swelling induced by hydrogen bonding: accurate prediction of swelling states. Langmuir, 22, 1223–1234.
Tamura, K., Yamada, H., and Nakazawa, H. (2000) Stepwise hydration of high-quality synthetic smectite with various cations. Clays and Clay Minerals, 48, 400–404.
Van Olphen, H. (1965) Thermodynamics of interlayer adsorption of water in clays. Journal of Colloid Science, 20, 822–837.
Van Olphen, H. and Fripiat, J.J. (1979) Data handbook for clay minerals and other non-metallic minerals, 346 p. Pergamon Press, New York.
Watanabe, T. and Sato, T. (1988) Expansion characteristics of montmorillonite and saponite under various relative humidity conditions. Clay Science, 7, 129–138.
Wilson, J., Cuadros, J., and Cressey, G. (2004) An in situ time-resolved XRD-PSD investigation into Na-Montmorillonite interlayer and particle rearrangement during dehydration. Clays and Clay Minerals, 52, 180–191.
Yamada, H., Nakazawa, H., Hashizume, H., Shimomura, S., and Watanabe, T. (1994) Hydration behavior of Na-smectite crystals synthetised at high pressure and high temperature. Clays and Clay Minerals, 42, 77–80.
Zabat, M. and Van Damme, H. (2000) Evaluation of the nergy barrier for dehydration of homoionic (Li, Na, Cs, Mg, Ca, Ba, $Al_x(OH)_y^{z+}$ and La)-montmorillonite by a differentiation method. Clay Minerals, 35, 357–363.

Manuscript received July 25, 2006
Manuscript accepted March 2, 2007
Manuscript handled by Warren Huff